nature structural & molecular biology

Quaternary contact in the initial interaction of CD4 with the HIV-1 envelope trimer

Qingbo Liu[1,5], Priyamvada Acharya[2,3,5], Michael A Dolan[4], Peng Zhang[1], Christina Guzzo[1], Jacky Lu[1], Alice Kwon[1], Deepali Gururani[1], Huiyi Miao[1], Tatsiana Bylund[2], Gwo-Yu Chuang[2], Aliaksandr Druz[2], Tongqing Zhou[2], William J Rice[3], Christoph Wigge[3], Bridget Carragher[3], Clinton S Potter[3], Peter D Kwong[2] & Paolo Lusso[1]

Binding of the gp120 envelope (Env) glycoprotein to the CD4 receptor is the first step in the HIV-1 infectious cycle. Although the CD4-binding site has been extensively characterized, the initial receptor interaction has been difficult to study because of major CD4-induced structural rearrangements. Here we used cryogenic electron microscopy (cryo-EM) to visualize the initial contact of CD4 with the HIV-1 Env trimer at 6.8-Å resolution. A single CD4 molecule is embraced by a quaternary HIV-1–Env surface formed by coalescence of the previously defined CD4-contact region with a second CD4-binding site (CD4-BS2) in the inner domain of a neighboring gp120 protomer. Disruption of CD4-BS2 destabilized CD4-trimer interaction and abrogated HIV-1 infectivity by preventing the acquisition of coreceptor-binding competence. A corresponding reduction in HIV-1 infectivity occurred after the mutation of CD4 residues that interact with CD4-BS2. Our results document the critical role of quaternary interactions in the initial HIV-Env-receptor contact, with implications for treatment and vaccine design.

The native HIV-1 Env spike on the surface of mature virions mediates viral attachment and entry[1], and it thus represents the major target for neutralizing antibodies and a central focus for vaccine development. The native spike is a trimer of gp120–gp41 heterodimers constrained into a metastable structure that is able to evade immunologic control by a variety of mechanisms, including antigenic variability, *N*-linked glycosylation, and conformational masking of the conserved receptor-binding sites[2,3]. Upon binding to the primary cellular receptor, CD4, the external gp120 Env glycoprotein undergoes major conformational changes, transitioning to a state that is competent for interaction with the CCR5 or CXCR4 coreceptor[1]. The CD4-binding site (CD4-BS) of gp120, which is a critical target for broad-spectrum neutralizing antibodies, has been finely mapped by both mutagenesis[4–7] and co-crystallization in complex with soluble CD4 (sCD4)[8–11]. However, most of those studies were performed with monomeric gp120 subunits, which hindered evaluation of the role of quaternary elements assembled in the pre-fusion trimeric structure that may be involved in the initial CD4 interaction. Quaternary interactions with an adjacent gp120 protomer have indeed been documented for two monoclonal antibodies (mAbs) directed to the CD4 supersite, VRC-PG04 (ref. 12) and VRC01 (ref. 13), by cryo-EM and crystallography, respectively. In addition, Lyumkis and colleagues[12] used *in silico* docking to model quaternary trimer interactions for additional anti-CD4-BS mAbs and for sCD4 itself, thereby predicting contacts of VRC01 and sCD4 with a limited surface of the α0 helix of an adjacent protomer, as well as more extensive contacts of other mAbs with basic residues in C2 and the V3 loop; however, they did not investigate the functional significance of these interactions.

Considerable progress has recently been made in the elucidation of the molecular anatomy of the HIV-1 Env spike, particularly with the design and crystallization of soluble truncated trimers (SOSIP.664) stabilized in a near-native configuration[13–18] and with the increasing resolution of cryo-EM imaging of native, membrane-bound Env spikes[19–21]. Nevertheless, it has remained challenging to obtain structural information on the initial contact of CD4 with the pre-fusion trimer, primarily because of the rapid transition of the trimer toward an open configuration after interaction with CD4 (ref. 22). Accordingly, cryo-EM studies have visualized the adoption of an open conformation by both soluble and membrane-bound Env trimers upon CD4 binding, regardless of the presence of bound antibodies directed to CD4-induced epitopes[21,23] or to epitopes compatible with the prefusion trimer state[24].

Here we present the cryo-EM structure of a conformationally constrained HIV-1 Env soluble trimer complexed with sCD4 and a trimer-specific broadly neutralizing antibody, PGT145, and document the quaternary configuration of the initial CD4-contact site in the closed, pre-fusion HIV-1 Env trimer. We show that the quaternary interactive site stabilizes CD4-Env binding and plays an essential role in HIV-1 entry into host cells, as its disruption prevents the acquisition of coreceptor-binding competence. Finally, we refine the boundaries of the CD4 antigenic supersite, and show that the quaternary CD4-interactive surface is immunogenic *in vivo*. These results have implications for HIV-1 treatment and vaccine design.

[1]Laboratory of Immunoregulation, National Institute of Allergy and Infectious Diseases, NIH, Bethesda, Maryland, USA. [2]Vaccine Research Center, National Institute of Allergy and Infectious Diseases, NIH, Bethesda, Maryland, USA. [3]National Resource for Automated Molecular Microscopy, Simons Electron Microscopy Center, New York Structural Biology Center, New York, New York, USA. [4]Bioinformatics and Computational Biosciences Branch, National Institute of Allergy and Infectious Diseases, NIH, Bethesda, Maryland, USA. [5]These authors contributed equally to this work. Correspondence should be addressed to P.L. (plusso@niaid.nih.gov).

Received 3 October 2016; accepted 25 January 2017; published online 20 February 2017; corrected after print 27 April 2017; doi:10.1038/nsmb.3382

RESULTS

Cryo-EM structure of initial CD4 contact with the HIV-1 Env trimer

To gain structural insights into the initial interaction of CD4 with the HIV-1 Env trimer, we used a conformationally constrained soluble trimer, DS-SOSIP.664 (ref. 16), which remains in a pre-fusion, closed conformation even after interaction with CD4, as evidenced by retention of binding to trimer-specific antibodies, including the V1V2 loop-directed mAb PGT145 (ref. 25). Notably, the DS-SOSIP.664 trimer binds sCD4 with an asymmetric 1:1 (CD4:trimer) stoichiometry[16], which probably reflects the earliest Env-receptor interaction. Thus, we formed complexes between DS-SOSIP.664, four-domain sCD4, and the antigen-binding fragment (Fab) of PGT145, and collected cryo-EM data, which yielded a 6.8-Å-resolution reconstruction (**Fig. 1a**,**b**, **Table 1**, and **Supplementary Figs. 1** and **2**). We used known structures of the Env trimer, sCD4, and PGT145 to position each molecule in the cryo-EM map (**Supplementary Tables 1** and **2**, and **Supplementary Fig. 2**), and we then minimized the Env-interactive interfaces with PGT145 and CD4. Because 6.8-Å resolution does not allow for experimental determination of residue side chains, we deposited coordinates with all residues truncated down to their Cβ atoms (PDB 5U1F).

The reconstructed map confirmed that the trimer was in a pre-fusion, closed conformation and was bound to a single CD4 molecule. The integrity of the pre-fusion trimer structure was reinforced by the presence of the quaternary-specific mAb PGT145, with its extended third heavy chain complementarity-determining region (CDR H3) loop penetrating through the glycan shield and reaching into a hole at the trimer apex formed by the junction of the V1V2 loops, making contacts with all three gp120 protomers, including the apex glycans, and essentially sealing the pre-fusion trimer at its apex (**Fig. 1a**,**c** and **Supplementary Fig. 2**). The highly electronegative CDR H3 loop of PGT145 lodged within an electropositive pocket formed by residues from all three protomers, with a sulfated tyrosine at its tip reaching into a space often occupied by SO_4^{-2} anions in previously reported structures of the pre-fusion closed trimer[13,15,16,18] (**Fig. 1c**).

Initial contact of CD4 with a quaternary Env surface

The reconstructed cryo-EM structure of the DS-SOSIP.664 trimer showed domain 1 of sCD4 inserted between two gp120 protomers to establish contacts not only with the previously defined CD4-BS in the outer domain of one gp120 protomer (hereinafter referred to as the primary CD4-contacting protomer), but also with CD4-BS2 in

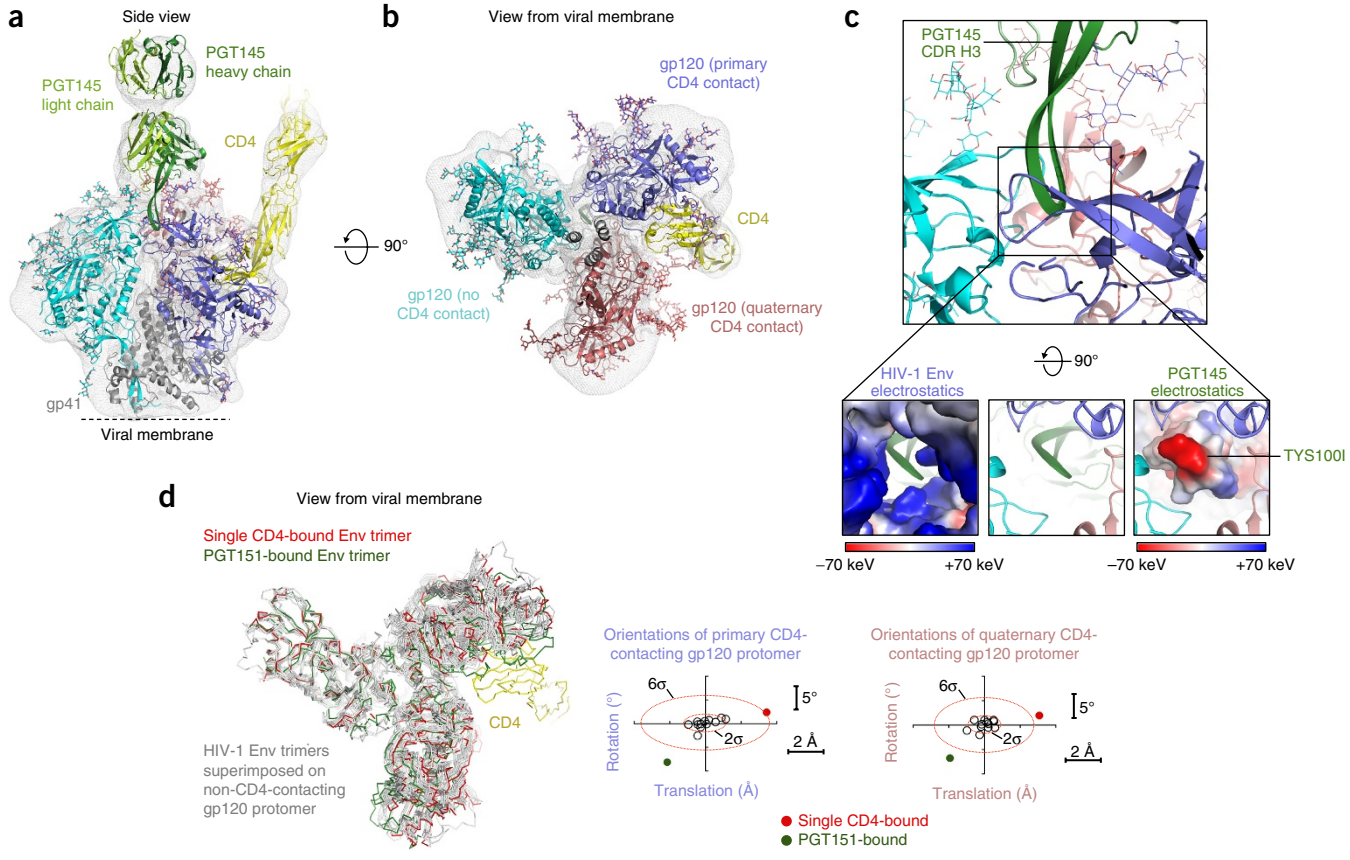

Figure 1 Cryo-EM structure of the initial interaction between the HIV-1 Env trimer and the CD4 receptor. (**a**) Side view of the cryo-EM structure of a ternary complex comprising DS-SOSIP HIV-1 Env trimer, four-domain sCD4 (yellow), and Fab from the broadly neutralizing mAb PGT145 (green), all shown in ribbon representation, with a 6.8-Å-resolution electron-microscopy-reconstructed density shown as a gray mesh. Each gp120 protomer is displayed in a different color, with gp41 in gray. (**b**) View from the viral membrane of the complex in **a** rotated 90°. CD4 contacts two gp120s, indicated as primary and quaternary CD4-contacting protomers, but not the third gp120. (**c**) Zoomed-in view of the PGT145 interaction. The images at the bottom show a 90° view (middle) and electrostatic surface display for HIV-1 Env (left) and for PGT145 (right). (**d**) Orientation of Env protomers in the prefusion, closed Env conformation recognized by a single CD4, displayed on the Env trimer in ribbon representation (left). Trimeric Env structures were aligned to the noncontacting protomer of the single CD4-bound trimer, and the resulting orientations of the primary and quaternary CD4-contacting protomers were plotted (right). The distance and angular measurements are absolute values measured from the single CD4-bound trimer. With asymmetric trimers, such as the PGT151-bound trimer (PDB 5FUU), each protomer was aligned to the noncontacting protomer of the single CD4-bound trimer, and the alignment displayed is the orientation with median positional displacement relative to the primary CD4-contacting protomer.

the inner domain of a neighboring protomer (quaternary CD4-contacting protomer), with no interactions with the third (non-CD4-contacting) protomer (**Fig. 1b**).

To define the orientations of the three Env protomers in the single CD4-bound closed trimer structure, we compared the orientation of each protomer in our reconstructed electron microscopy map with those in previously determined structures of the pre-fusion closed Env trimer (**Supplementary Table 1**). We superimposed the structures by aligning each previously defined protomer onto the coordinate model of the non-CD4-contacting protomer in our cryo-EM reconstruction, and compared the resulting orientations of the other two protomers (**Fig. 1d**). We found the position of the primary CD4-contacting protomer in our structure to be shifted by an average translation of 3.4 Å and a rotation of 2.4° relative to the mean coordinate position of other pre-fusion soluble trimer structures, whereas the quaternary CD4-contacting protomer shifted by a translation of 3.1 Å and a rotation of 1.9°, with both protomers moving outward from the trimer axis toward the CD4 molecule (**Fig. 1d**). The most distal orientation for both primary (difference of 5.6 Å translation and 10.5° rotation) and quaternary (difference of 5.0 Å translation and 8.7° rotation) CD4-contacting protomers occurred with the PGT151 complex[20], which also induces an asymmetric conformation, but in the opposite direction. We did not observe any major change in the secondary structure of either gp120 or gp41 in the 6.8-Å map versus prior pre-fusion closed structures, which reflects the ability of the HIV-1 Env protomers to sustain movements of up to 5 Å without undergoing substantial structural rearrangements. Although the 6.8-Å resolution of the reconstructed cryo-EM map precluded experimental definition of individual side chain positions, robust fits of the Env protomer domains to the reconstructed electron microscopy map (**Fig. 1a**,**b** and **Supplementary Table 1**), together with a statistically significant difference of domain orientations of 6σ or greater relative to the population of trimer structures shown in gray in **Figure 1d**, allowed for the positioning of an asymmetric protomer domain arrangement within the single CD4-bound trimer structure.

To obtain insights into the CD4-trimer interaction, we used a molecular dynamics (MD) simulation that led us to focus on four candidate CD4-contacting residues in the quaternary CD4-contacting protomer, namely, E62, E64, and H66 in the αĪ-helix, and K207 at the base of the β3-β4 loop (**Fig. 2a**). In the crystal structure of the unliganded trimer[18], the side chains of these residues project toward the incoming CD4 receptor and are exposed to the solvent (**Fig. 2a**). Notably, residues E64, H66, and K207 are nearly universally conserved (>99.7%) across all group M HIV-1 isolates, whereas position 62 is occupied by an acidic residue (E or D) in more than 90% of group M isolates (**Fig. 2b**).

Critical role of quaternary CD4 interaction in HIV-1 infection

To elucidate the functional relevance of the quaternary CD4 contact to HIV-1 infection, we mutagenized residues E62, E64, H66, and K207 in full-length gp160 from six HIV-1 isolates of different genetic subtypes—namely, BG505 (clade A), BaL and JR-FL (clade B), ZM106.9 (clade C), QD435.A4 (clade D), and CM244 (clade E)—and generated infectious viral pseudoparticles for each mutant. We introduced both individual and combined charge inversions into each Env to create a reverse-charged surface; for the control condition, we mutated by charge inversion a key residue in the primary CD4-BS, D368 (refs. 5,26). Both wild-type and mutated gp160 were efficiently expressed on the surface membrane of transfected human embryonic kidney (HEK) 293T cells and did not show alterations in their folding and trimeric structure, as determined by reactivity with a wide panel of anti-envelope mAbs, including trimer-preferring and cleavage-sensitive mAbs such as PG9 (ref. 27), 35O22 (ref. 28), and PGT151 (ref. 20) (**Supplementary Table 3**). Charge inversions of E62, E64, H66, and K207 virtually abrogated the infectivity of all of the HIV-1 Env types tested, regardless of their genetic clades, as did the control D368R mutation (**Fig. 2c**,**d**).

We introduced a set of additional mutations into the BaL Env to obtain a more complete topological and functional mapping of the CD4-BS2 region. Alanine substitutions of E62, E64, H66, and K207, either individually or in combination, consistently reduced HIV-1 infectivity, albeit less markedly than charge inversions; nevertheless, a triple-alanine substitution (D62A, E64A, and K207A) caused a complete loss of infectious capacity (**Supplementary Fig. 3**). Charge inversions or alanine substitutions of neighboring solvent-exposed residues either had no effects (K59E, E102A, or E102K) or enhanced infectivity (Y61A, presumably owing to removal of the bulky side chain, which allowed for closer approach of CD4 to CD4-BS2), thus corroborating the specificity of the effects observed upon disruption of CD4-BS2. These results suggest a critical role of the quaternary trimer interaction with CD4 for the progression of the HIV-1 fusogenic process.

Table 1 Cryo-EM data collection and refinement information

	DS-SOSIP.664-sCD4-PGT145 (EMD-8427)
Data collection	
Software	Leginon 3.1
Pixel size (Å)	1.1
Defocus range (μm)	1.0–4.0
Voltage (kV)	300
Electron dose (e^{-}/Å^2)	86
Magnification	22,500
Refinement	
Software	RELION 1.4
Particles	55,000
Resolution (Å)	6.8
Accuracy of rotation (°)	4.63
Accuracy of translation (pixels)	2.81
Map-sharpening *B*-factor (Å^2)	–172

Stabilization of CD4 binding to the trimer by quaternary interaction

To elucidate the mechanism underlying the complete loss of infectivity induced by disruption of CD4-BS2, we initially tested whether the mutations caused reduced gp120-gp41 association, but the levels of gp120 shedding from cell-surface-expressed gp160 were unaltered (data not shown). Next, we mutagenized the four CD4-BS2 residues (E62, E64, H66, and K207) in both the DS-variant and wild-type soluble SOSIP trimers and measured the ability of the mutants to bind sCD4. The trimers were expressed in HEK293 free-style (FS) cells and purified to homogeneity (**Supplementary Fig. 4**). As expected from the outward orientation and complete solvent exposure of the side chains of the CD4-BS2 residues, their mutation by simple charge inversion had no effect on the correct folding and trimeric configuration of the mutants, as shown by reactivity with a panel of mAbs that included several trimer-preferring, conformation-dependent and cleavage-sensitive mAbs (**Supplementary Fig. 4a**). Surface plasmon resonance (SPR) analysis showed that all of the DS-SOSIP-based CD4-BS2 mutants had markedly reduced sCD4-binding affinity (K_D), which was primarily due to an accelerated off-rate, with K207E exhibiting the most pronounced decrease (K_D = 262.0 nM, compared to

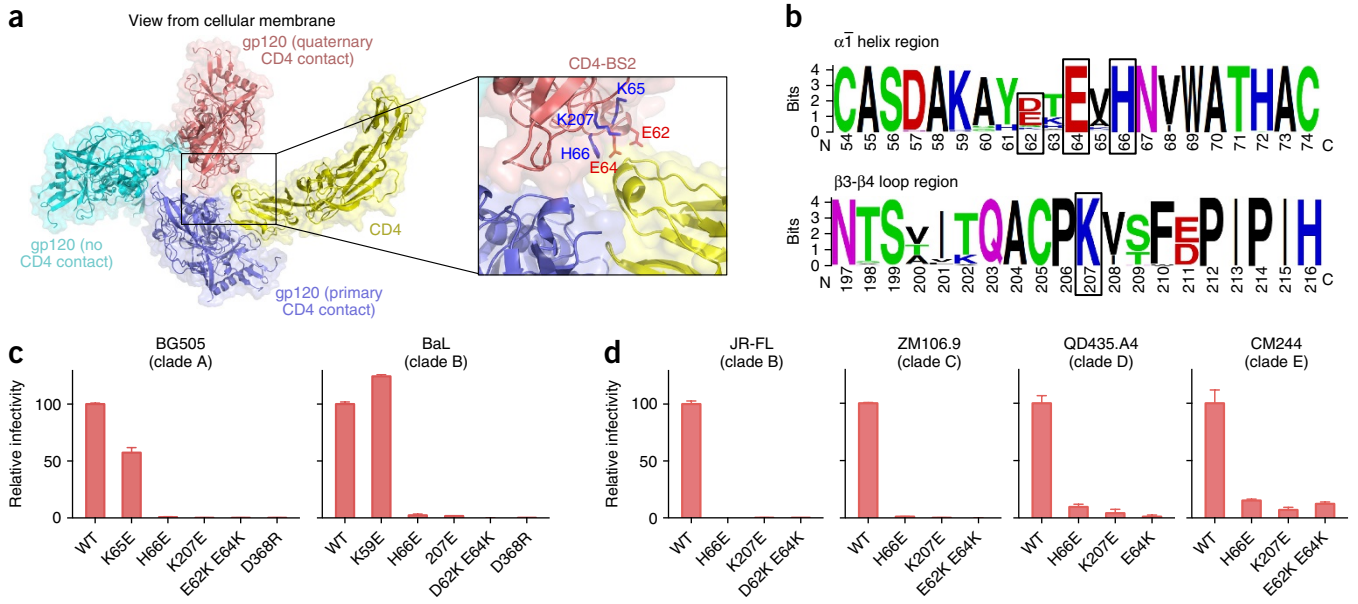

Figure 2 Quaternary configuration of the CD4-binding site in the initial interaction with the HIV-1 Env trimer. (**a**) Top view of the cryo-EM structure of an HIV-1 Env trimer bound to a single CD4 receptor showing the quaternary interaction of CD4 (yellow) with two neighboring gp120 protomers; gp41 was removed for clarity. The image on the right shows a close-up view of the CD4-binding site (CD4-BS2) on the quaternary contacting gp120. Residues in the C1 (α1-helix) and C2 (β3-β4 loop) regions of the quaternary CD4-contacting gp120 protomer (pink) are highlighted in stick representation (E62 and E64, negatively charged; H66 and K207, positively charged). The location of K65, which points away from CD4, is shown for reference. (**b**) Amino acid conservation within the CD4-BS2 region. Residues E64, H66, and K207 are nearly universally conserved (>99.7%) across all group M HIV-1 isolates; position 62 is occupied by an acidic residue (either E or D) in more than 90% of group M isolates, with nonconservative mutations essentially limited to genetic subtype D (58% E→K) and subtypes G and J (100% E→S). (**c**) Disruption of CD4-BS2 by charge inversion abrogates HIV-1 infectivity. Infectious pseudoparticles bearing wild-type (WT) or mutated BG505-T332N (clade A) or BaL (clade B) Env were tested in TZM-bl cells. Infectivity values for each mutant were calculated relative to the value obtained for the wild type. (**d**) Infectivity of viral pseudotypes carrying mutated HIV-1 Env from different genetic subtypes. The infectivity of each mutant was calculated relative to that of the respective wild-type Env. The data shown in **c** and **d** represent mean ± range of duplicate wells from a representative experiment out of three performed that yielded similar results.

8.0 nM for the unmutated DS-SOSIP), followed by H66E (K_D = 127.2 nM) and E62K E64K (K_D = 57.7 nM); no detectable binding was seen with the control D368R mutant (**Fig. 3a**). Likewise, all the wild-type-based mutants showed a similarly reduced ability to bind sCD4 in both ELISA (**Supplementary Fig. 5a**) and SPR assays (**Fig. 3b**), thus excluding the possibility that the reduced CD4-binding affinity could be specific for the stabilized DS-SOSIP trimer. Because soluble SOSIP trimers display some structural and antigenic differences from native Env trimers[29], we also tested CD4 binding to full-length native gp160 expressed on the surface membrane of HEK293T cells. All CD4-BS2 mutants for both BG505 and BaL Env exhibited reduced binding to CD4–immunoglobulin compared with the respective wild-type proteins (**Supplementary Fig. 5b**). Together, these results demonstrate that CD4-BS2 has an important role in stabilizing the interaction of the HIV-1 Env trimer with CD4.

Quaternary CD4 interaction confers coreceptor-binding competence

Next we studied the events downstream of CD4 binding, which induce gp120 to acquire coreceptor-binding competence and eventually to dissociate from gp41, thus leading to activation of the fusogenic process. After preactivation with sCD4, the BG505 SOSIP.664 soluble trimer efficiently bound to cell-surface-expressed CCR5; in contrast, none of the CD4-BS2 mutants were able to bind to CCR5 regardless of sCD4 treatment (**Fig. 3c**). Likewise, little, if any, induction of the 48d epitope, which extensively overlaps the CCR5-binding surface[30], was detected in any of the CD4-BS2 mutants after treatment with sCD4 (**Fig. 3d**). These results indicate that the quaternary interaction of CD4 with the gp120 inner domain is essential for the conformational transitions that lead to coreceptor binding and progression of the fusogenic process.

Limited effects of CD4-BS2 mutagenesis on monomeric gp120

As mutation of specific residues in the gp120 inner domain, including H66, was previously reported to reduce the binding of sCD4 and coreceptors to monomeric gp120 (refs. 7,31), we investigated the effects of CD4-BS2 mutations in the context of gp120 monomers. We confirmed the correct folding of the mutated gp120 proteins on the basis of their reactivity with a panel of mAbs to gp120 (**Supplementary Fig. 6**). Among all mutants, only H66E showed a slight reduction in sCD4-binding activity in both BG505 and BaL gp120, whereas K207E showed reduced binding only in BG505 and not in BaL gp120 (**Supplementary Fig. 6a**), indicating that CD4-BS2 is not a functionally relevant receptor-binding site in the context of the monomer. Mutation of CD4-BS2 residues resulted in decreased CCR5 and 48d binding in the absence of sCD4 (**Supplementary Fig. 6b**), which confirmed the findings of previous mutagenesis studies that attributed this effect to reduced monomer flexibility caused by altered interlayer interactions in the inner domain[7,31]. In contrast, in the presence of sCD4, binding of 48d was unaffected by CD4-BS2 mutations, which shows that sCD4 was able to induce the full range of conformational changes in the context of the mutated monomer, whereas binding to CCR5 was only moderately reduced, with the exception of mutant K207E that, as expected, lost the ability to bind CCR5, as this residue

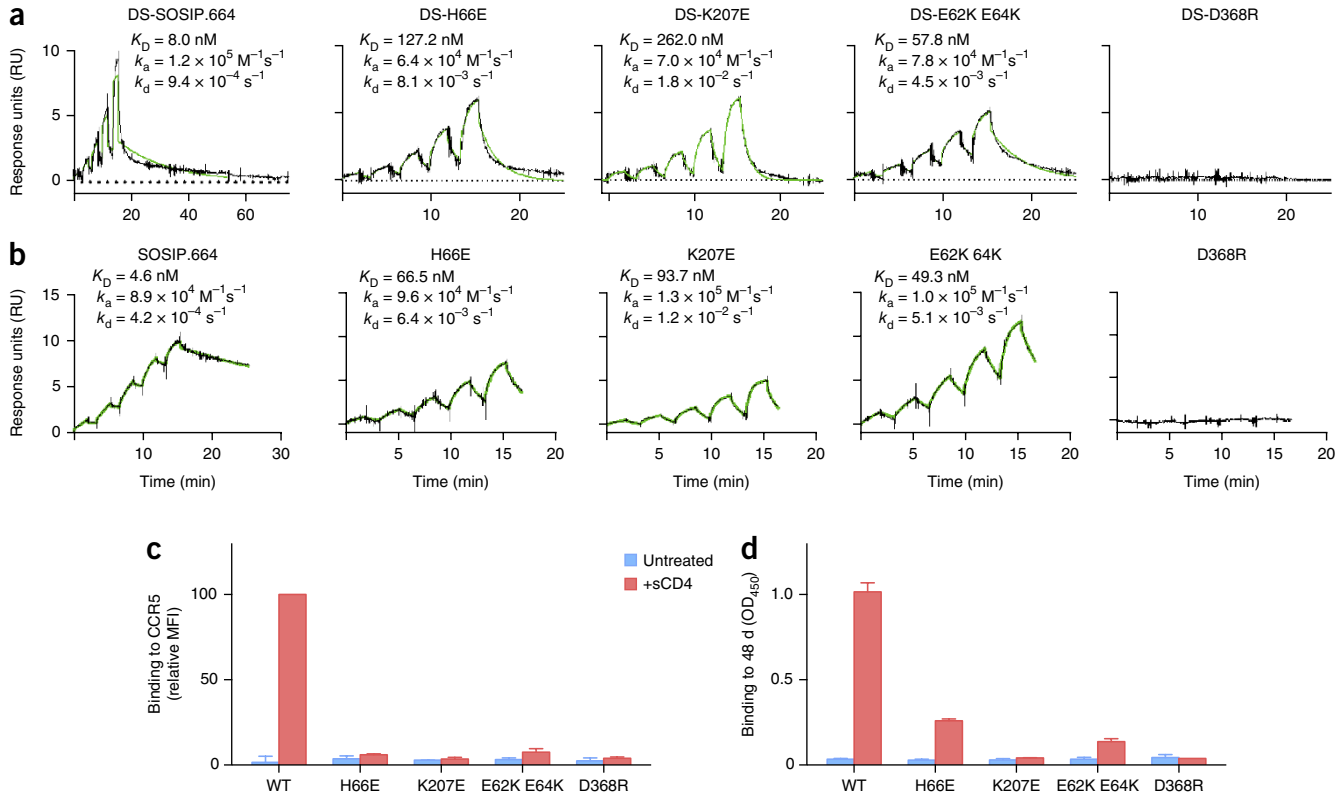

Figure 3 Charge inversions in CD4-BS2 reduce the CD4-binding capacity of the BG505 SOSIP.664 trimer. (**a**) The kinetics of sCD4 binding to the DS-SOSIP-based trimers as measured by single-cycle SPR. (**b**) The kinetics of sCD4 binding to wild-type and mutated trimers as measured by single-cycle SPR. (**c**) Charge inversions in CD4-BS2 abrogated the CCR5-binding capacity of BG505 SOSIP.664 trimers after sCD4 treatment. Binding of wild-type (WT) and mutated soluble BG505 SOSIP.664 trimers to CCR5 expressed on the surface of Cf2Th/syn-CCR5 cells was assessed by flow cytometry. Mean fluorescence intensity (MFI) values were calculated relative to the positive control (sCD4-bound wild-type trimer). The data shown represent the mean ± range of two independent experiments. (**d**) Charge inversions in CD4-BS2 abrogate the mAb 48d-binding capacity of BG505 SOSIP.664 trimers after sCD4 treatment, as assessed by ELISA. The data shown represent the mean ± range of duplicate wells from a representative experiment out of three performed that yielded similar results.

is part of the coreceptor-contact surface[32] (**Supplementary Fig. 6b**). Overall, the effects observed after mutation of monomeric gp120 were only partial and limited, unlike the complete loss of CCR5 and 48d binding observed in the context of the trimer (**Fig. 3c**,**d**).

To interpret the above results, we examined the available crystal structures of monomeric gp120, which invariably revealed a disassembled CD4-BS2 region attributable to the opposite spatial orientation of the E62, E64, H66, and K207 side chains, which in the monomer point inward to establish intramolecular contacts with residues in the underlying layer 2 of the gp120 inner domain[8–11]; conversely, in the structures of soluble Env trimers, the same residues point outward to form a continuous, electrostatically charged surface crest[13,16–18] (**Supplementary Fig. 7**). Thus, as previously suggested[7,31], the slight reduction of CD4 and CCR5 binding observed in the context of monomeric gp120, as well as the reduced binding of mAb 48d in the absence of sCD4, may have been due to reduced molecular flexibility and distant allosteric effects secondary to altered interlayer adherence in the flexible inner domain of the gp120 glycoprotein.

Identification of CD4 residues involved in quaternary interaction

To further validate the role of CD4-BS2 in the HIV-1 envelope-receptor interaction, we investigated the CD4 residues that make contact with CD4-BS2 (**Fig. 4a**). On CD4, two discontinuous surfaces mirror the quaternary binding site on the Env trimer, with one surface interacting with the primary CD4-contacting protomer, and the other interacting with the quaternary CD4-contacting protomer (**Fig. 4b**). To estimate the surface areas of interaction, we used previously determined coordinates of Env trimers and two-domain sCD4 (residues 1–176) fitted to the electron microscopy density (**Fig. 4c** and **Supplementary Table 2**). Fittings of CD4 to the reconstructed cryo-EM map revealed an ~6-Å translation and an ~8° rotation for the median position of CD4 in the initial contact structure relative to the position of CD4 in the monomeric postfusion structure. A total of 7 Env trimers and 29 CD4 domains produced a matrix of 203 interactive surfaces, yielding 526 ± 52 Å^2 of buried surface area for the primary CD4-contacting gp120, and 159 ± 41 Å^2 of buried surface area for the quaternary CD4-contacting gp120 (**Supplementary Table 4**). Examination of the contact site in the fitted model and in the MD simulation revealed four residues in CD4 domain 1, namely, $K21_{CD4}$ and $K22_{CD4}$ in the CDR1-like loop, and $D63_{CD4}$ and $Q64_{CD4}$ in the D-E loop, as potentially interactive with CD4-BS2 in the fitted cryo-EM structure and in the MD simulation; none of these residues had been previously reported to contact gp120 (refs. 8–11).

To assess the functional role of the CD4 residues predicted to interact with CD4-BS2, we mutagenized each residue by charge inversion, expressed full-length CD4 mutants on the surface of Cf2Th/syn-CCR5 cells, and tested the mutants for HIV-1 receptor function. We verified the correct expression and folding of the mutants with a panel of mAbs to CD4 (**Supplementary Fig. 8**); of note, mAbs RPAT4, 13B8, and 379 showed a significant loss of reactivity with mutant $K22E_{CD4}$, which

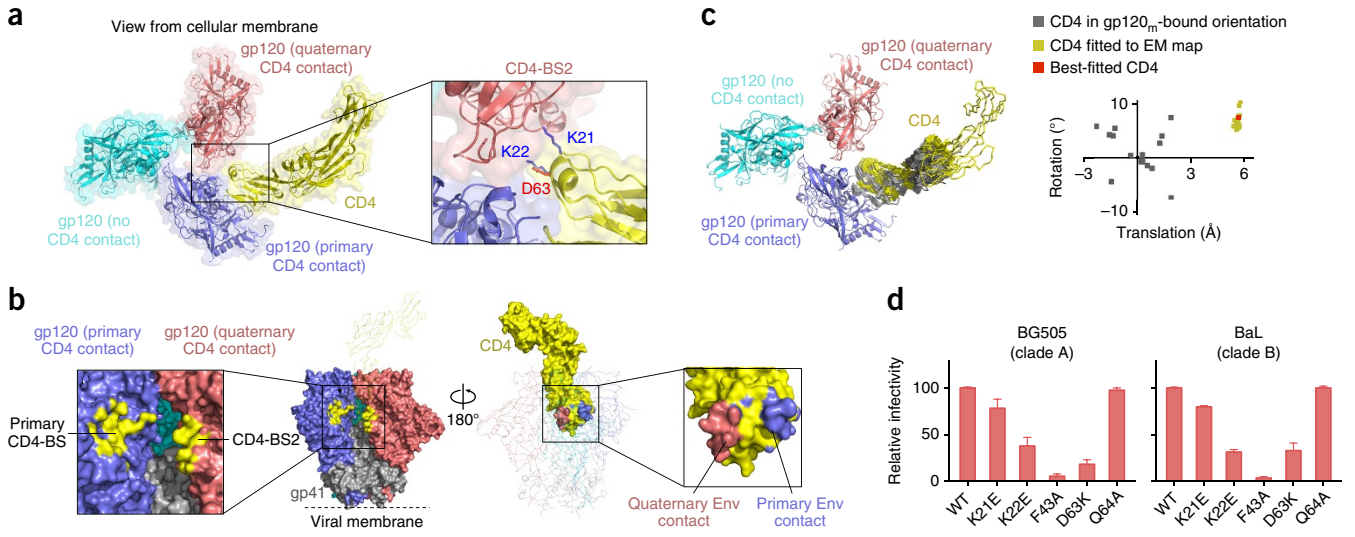

Figure 4 CD4 surface interacting with CD4-BS2 in the initial contact with Env. (**a**) Left, top view of the cryo-EM structure of a single-CD4-bound HIV-1 Env trimer, showing the quaternary interaction of CD4 with neighboring gp120 protomers; gp41 was removed for clarity. Right, a close-up representation of CD4 residues (highlighted by stick representation and color) at the interface with CD4-BS2 in gp120 (D63, negatively charged; K21 and K22, positively charged). (**b**) Open-book surface representations of the quaternary HIV-1 Env–CD4 interaction in the optimized cryo-EM structure. The CD4 footprint on the HIV-1 Env trimer is shown in yellow, and the trimer footprints on CD4 are shown in purple for the primary CD4-contacting gp120 and in pink for the quaternary CD4-contacting gp120. Zoomed-in views show the contact sites (within 5.5 Å). (**c**) Left, top view of the cryo-EM structure of a single-CD4-bound HIV-1 Env trimer, showing CD4 molecules fitted into the cryo-EM density map (yellow) and CD4 molecules in the monomeric gp120 ($gp120_m$)-bound (postfusion) orientation (listed in **Supplementary Table 2**) (gray). CD4 fits were performed with CD4 domains 1 and 2; CD4 domains 3 and 4 were added to the CD4 molecule showing the best fit by alignment with four-domain CD4 (PDB 1WIO) and by transplantation of domains 3 and 4 onto fitted domains 1 and 2. Gp41 was removed for clarity. Right, orientation of the CD4 molecules fitted into the cryo-EM density map relative to the $gp120_m$-bound orientation. "Best-fitted CD4" refers to the CD4 fit that was chosen for the final DS-SOSIP-CD4-PGT145 model fitted to the cryo-EM density. This fit showed the highest map-to-model correlation among all the CD4 molecules. (**d**) Disruption of the CD4-BS2 interactive site reduces the HIV-1 receptor function of CD4. Pseudoviruses carrying wild-type (WT) BG505-T332N or BaL envelopes were tested for infectivity in Cf2Th/syn-CCR5 cells expressing different CD4 mutants. Infectivity values for the mutants were calculated relative to the value obtained with wild-type CD4. The data shown represent the mean ± range of duplicate wells from a representative experiment out of two performed that yielded similar results.

suggests that the mutations directly overlap their binding footprint or, less likely, that charge inversion may have caused subtle conformational changes. Charge inversion of two CD4 residues, $K22_{CD4}$ and $D63_{CD4}$, caused a dramatic loss of HIV-1 receptor function, as seen with both the BG505 and BaL envelopes, whereas charge inversion of $K21_{CD4}$ had more limited effects, and alanine substitution of $Q64_{CD4}$ had no effects; as expected, alanine substitution of the critical $F43_{CD4}$ residue caused a complete loss of receptor function (**Fig. 4d**). Analysis of a more extended panel of CD4 mutants showed that alanine substitutions of $K22_{CD4}$ and $D63_{CD4}$ also reduced HIV-1 infectivity, albeit less markedly than charge inversions (**Supplementary Fig. 8a**). These results confirmed that alterations on both sides of the CD4:CD4-BS2 interface disrupt the functional interaction between the HIV-1 envelope and the CD4 receptor.

Role of quaternary interaction in neutralizing antibody binding

To assess the immunogenicity of CD4-BS2 and its functional relevance to antibody-mediated neutralization and immune evasion, we examined the potential interaction of this site with a panel of anti-CD4 supersite mAbs isolated from HIV-1-infected individuals. Numerous structures of these mAbs have been determined in complex with monomeric gp120 (refs. 33–37) and in the context of the Env trimer[12,13]. Docking onto the pre-fusion closed Env trimer revealed that all of the anti-CD4 supersite mAbs reach deep into the interprotomer groove, although only some of them (most notably VRC03, VRC06, and VRC-CH31) appear to make direct contact with CD4-BS2 (**Fig. 5a**). Optimization of quaternary contacts appeared to occur by somatic hypermutation-induced alteration of the framework regions of these antibodies (**Supplementary Fig. 9**). We note that quaternary interactions were predicted for several anti-CD4 supersite antibodies, including VRC01 (ref. 12), and the crystal structure of the VRC01-bound X1193.c1 SOSIP.664 trimer, but not of the JR-FL trimer, indeed documented quaternary contacts with residues Y61 and E64 in the gp120 inner domain[13]. These observations may relate to strain-specific modes of interaction between Env and broadly neutralizing antibodies.

Mutation of the key residues in CD4-BS2 had diverse effects on binding of anti-CD4 supersite mAbs to the BG505 SOSIP.664 trimer (**Fig. 5b**). Specifically, charge inversion of K207 substantially decreased recognition by VRC03 and, to a lesser extent, VRC-CH31 and 3BNC117, but not VRC06; in contrast, mutation of E62 E64 selectively affected VRC06 binding, whereas none of these mutations significantly reduced the binding of VRC01 and VRC-PG04. We confirmed these results with a more extended panel of mAbs and envelope mutants tested on cell-surface-expressed gp160 from both BG505 and BaL (**Supplementary Table 3**). In line with their dependence on CD4-BS2, and consistent with previous data[36], both VRC03 and VRC06 exhibited trimer-preferring reactivity, with no detectable binding to monomeric BG505 and BaL gp120 in ELISA (**Supplementary Fig. 6c**), even though binding and even crystallization in complex with monomeric gp120 have been reported for other strains[37,38]. Overall, these results demonstrate that certain neutralizing human mAbs establish quaternary contacts with the HIV-1 Env spike, and thus provide inferential evidence that the CD4-BS2 region is immunogenic *in vivo*.

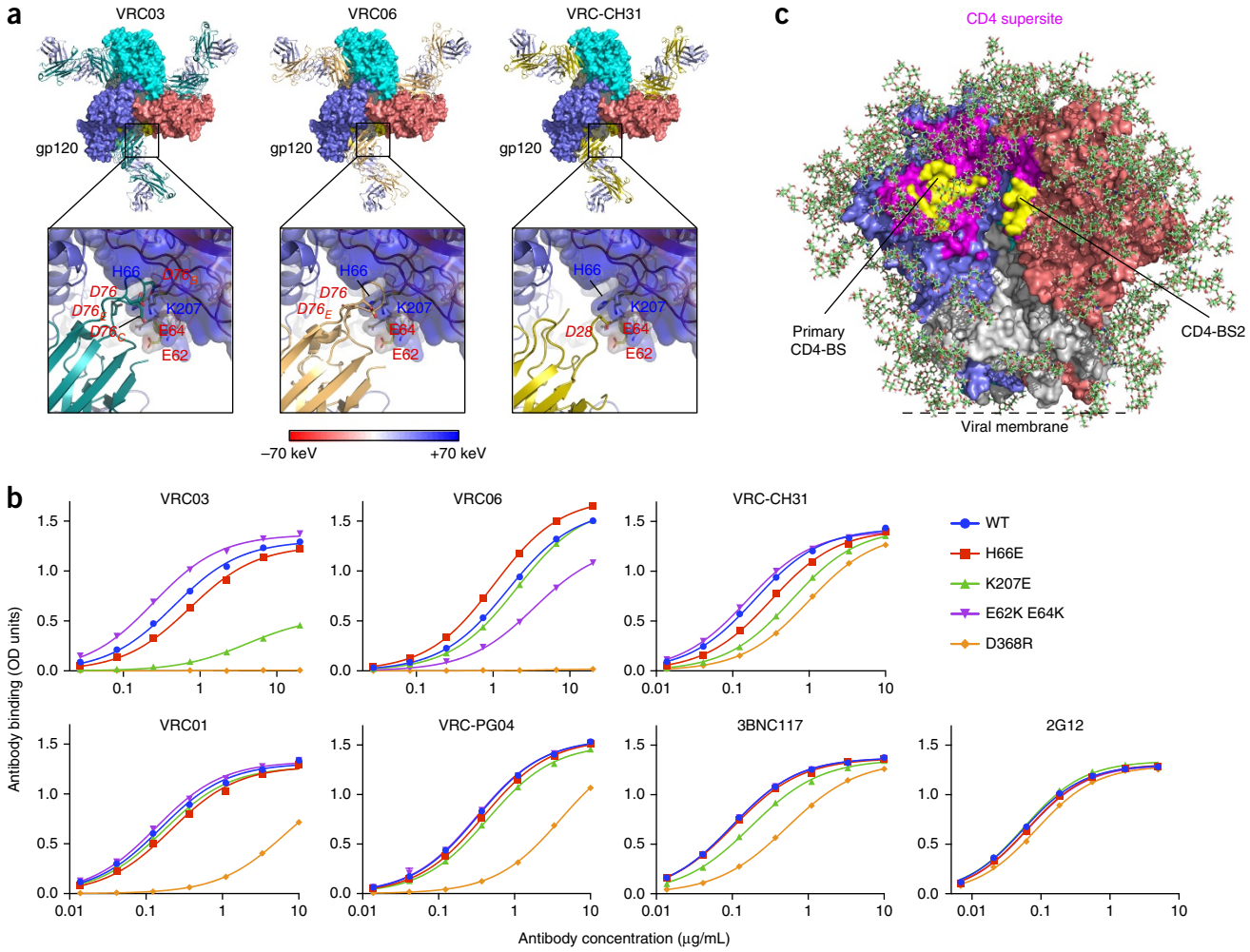

Figure 5 Quaternary interactions of selected antibodies to CD4-BS with the HIV-1 Env trimer. (**a**) Fabs for select neutralizing mAbs to CD4-BS (i.e., VRC03, VRC06, and VRC-CH31) are shown along the top, docked to a surface representation of the HIV-1 Env trimer in its pre-fusion closed conformation. The close-up views below show the putative contact area with CD4-BS2, with key residues (E62, E64, H66, and K207) highlighted by stick representation with Env colored by electrostatics. (**b**) Disruption of CD4-BS2 affects binding of neutralizing mAbs specific for the CD4-binding site. Binding of anti-CD4-BS mAbs to wild-type (WT) and mutated soluble cleaved HIV-1 Env trimers (BG505 SOSIP.664) as assessed by ELISA. The data shown represent the mean ± range of duplicate wells from a representative experiment out of two performed that yielded similar results. (**c**) A surface representation of the CD4 supersite of vulnerability, with CD4-contact sites highlighted in yellow. Glycans are shown in stick representation.

DISCUSSION

Our work delineates the initial contact of the HIV-1 Env with the CD4 receptor, documenting the quaternary configuration of a retrovirus receptor-binding site, a feature previously recognized for picornaviruses[39–41], but never before for enveloped viruses. We found that the initial CD4-binding site on the pre-fusion HIV-1 Env trimer spans conserved regions on two neighboring gp120 protomers, which embrace the receptor with an extended quaternary surface complementary to discontinuous elements located on two faces of the N-terminal domain of CD4. This initial interaction with CD4 represents the first event in a multistep process during which the trimer undergoes sequential structural transitions toward downstream intermediate states (i.e., a requisite intermediate high-FRET state[22], a three-CD4-bound state[21,42], and coreceptor-bound states[22,43]) before reaching a final, low-energy postfusion state[1–3]. To prevent CD4-induced conformational changes in the trimer, which until now have impeded the study of the initial events of receptor interaction, we took advantage of a conformationally stabilized soluble trimer, DS-SOSIP, which binds CD4 with an asymmetric 1:1 (CD4:trimer) stoichiometry[16]. Accordingly, our cryo-EM structure showed structural asymmetry in the initial Env–CD4 complex, with an ~3-Å outward shift of both CD4-interactive protomers toward the incoming CD4 molecule. This shift represents perhaps the earliest conformational change to take place in the HIV-1 Env trimer. Its marked asymmetry seems to be maintained in the requisite transition intermediate observed by smFRET[22], before binding of two additional CD4 molecules yields the 3:1 (CD4:trimer) stoichiometry commonly observed with the CD4-bound open trimer[21,23,42].

The dramatic loss of HIV-1 infectivity that we observed when we mutated key residues involved in the quaternary Env-CD4 contact both on the trimer and on the receptor sides indicates that binding to the full quaternary Env surface is critical for the functional interaction of CD4 with the HIV-1 virion. The more pronounced effect induced by charge inversion versus alanine mutagenesis suggests that CD4 interaction with CD4-BS2 is predominantly driven by electrostatic forces. The quaternary site in the inner gp120 domain appears to be essential to stabilize the Env-receptor interaction and to trigger Env activation, which in turn leads to coreceptor binding and progression of the

fusogenic process. In agreement with this model, the inner domain has been implicated in regulation of the transition from the pre-fusion ligand-free to the CD4-activated conformation in the context of monomeric gp120 (ref. 7). However, the orientation of the CD4-BS2 region is dramatically different in the trimer and the monomer. In the pre-fusion metastable trimer, the key residues that form CD4-BS2 point outward and are well exposed to the solvent, facing the incoming CD4 receptor; in contrast, the same residues display a peculiar inward orientation and are almost completely buried in the fusion-transitioned structure of the monomeric gp120 core[8–11]. Thus, in the context of the monomer only, CD4-BS2 residues establish intramolecular interactions with layer-2 residues, which affect interlayer adherence in the inner domain and, consequently, monomer flexibility and spontaneous access to the coreceptor-binding-competent state. This can explain the allosteric effects on CD4 binding that have been previously reported after mutation of H66 and other inner-domain residues in the context of the monomer[7,31]. The cryptic configuration of the CD4-BS2 region in monomeric gp120 also suggests that the quaternary CD4-contact site may be a region of conformational masking[3] that facilitates the immune evasion of this critical surface.

Major efforts aimed at developing a protective vaccine are currently focused on the design of HIV-1-Env-based immunogens that display the major epitopes recognized by broad and potent neutralizing antibodies[14,16,44]. The definition of the initial CD4-contact surface in the HIV-1 Env trimer allowed us to reassess the supersite of vulnerability formed by the CD4-binding site (**Fig. 5c**), with potential implications for the development of HIV-1 vaccines. Our observation that selected neutralizing antibodies to the CD4-BS, such as VRC03 and VRC06, which preferentially recognize the trimeric envelope, develop contact with CD4-BS2 through somatic hypermutation provides evidence that this region is immunogenic *in vivo* and, therefore, should be considered in the design of vaccine immunogens. Furthermore, the CD4-BS2 region may provide a new molecular target for the development of HIV-1 entry inhibitors.

METHODS

Methods, including statements of data availability and any associated accession codes and references, are available in the online version of the paper.

Note: Any Supplementary Information and Source Data files are available in the online version of the paper.

ACKNOWLEDGMENTS

We thank J.P. Moore and A. Cupo (Weill Medical College of Cornell University, New York, New York, USA) for providing plasmids for expression of the BG505 SOSIP.664 trimer and furin; M. Farzan (Scripps Research Institute, Jupiter, Florida, USA) for providing the plasmid to express human CD4-immunoglobulin; D.R. Burton (Scripps Research Institute, La Jolla, California, USA, and Ragon Institute of MGH, MIT and Harvard, Cambridge, Massachusetts, USA), M. Connors (Laboratory of Immunoregulation, NIAID, NIH, Bethesda, Maryland, USA), J.R. Mascola (Vaccine Research Center, NIAID, NIH, Bethesda, Maryland, USA), and J.E. Robinson (Tulane University School of Medicine, New Orleans, Louisiana, USA) for anti-gp120 mAbs; E. Berger (Laboratory of Viral Diseases, NIAID, NIG, Bethesda, Maryland, USA) for the full-length *CD4* gene and the gene encoding gp160 from BG505-T332N and BaL; D. Ichikawa and Y. Lin for help in performing selected experiments; J. Arthos, E.A. Berger, and R. Cimbro for helpful discussion; P. Gangopadhyay for help with MATLAB and Origin; and the AIDS Reagent Program for providing the reagents indicated in the Online Methods. The GPU-enabled frame-alignment program we used was generously provided by Y. Cheng and X. Li. The cryo-EM work was done at the National Resource for Automated Molecular Microscopy based at the Simons Electron Microscopy Center, which is supported by grants from the NIH (GM103310 and S10 OD019994-01) and the Simons Foundation (349247) to B.C. and C.S.P. This research was supported by the Intramural Programs of the Vaccine Research Center and of the Division of Intramural Research, NIAID, NIH.

AUTHOR CONTRIBUTIONS

Q.L. and P.L. conceived the project and designed biological and virological studies; P.A., T.Z., and P.D.K. conceived and designed structural studies; Q.L., J.L., and D.G. mutagenized gp160 from different HIV-1 isolates and produced infectious pseudoparticles; Q.L., C.G., H.M., and A.K. carried out infectivity assays and antigenicity studies of surface-expressed Envs; Q.L., D.G., and P.Z. produced and purified mutants of SOSIP trimer and gp120 monomer; Q.L. characterized the purified proteins and performed immunogenicity studies and CD4-binding and CCR5-binding assays; A.D. expressed DS-SOSIP proteins for SPR and cryo-EM studies; Q.L. and P.A. purified CD4-BS2 mutants of DS-SOSIP trimer and performed SPR analysis of CD4 binding; P.A. purified DS-SOSIP, prepared the DS-SOSIP-CD4-PGT145 complex, and performed cryo-EM experiments, with W.J.R. and C.W. providing assistance with electron microscopy data collection; P.A., T.B., G.-Y.C., and T.Z. analyzed the structure; M.A.D. performed docking experiments and MD simulations; B.C., C.S.P., and P.D.K. supervised cryo-EM experiments and structural analyses; Q.L., P.A., P.D.K., and P.L. analyzed data and wrote the paper; and all coauthors read and commented on the manuscript.

COMPETING FINANCIAL INTERESTS

The authors declare no competing financial interests.

1. Wyatt, R. & Sodroski, J. The HIV-1 envelope glycoproteins: fusogens, antigens, and immunogens. *Science* **280**, 1884–1888 (1998).
2. Mascola, J.R. & Haynes, B.F. HIV-1 neutralizing antibodies: understanding nature's pathways. *Immunol. Rev.* **254**, 225–244 (2013).
3. Kwong, P.D. *et al.* HIV-1 evades antibody-mediated neutralization through conformational masking of receptor-binding sites. *Nature* **420**, 678–682 (2002).
4. Lasky, L.A. *et al.* Delineation of a region of the human immunodeficiency virus type 1 gp120 glycoprotein critical for interaction with the CD4 receptor. *Cell* **50**, 975–985 (1987).
5. Olshevsky, U. *et al.* Identification of individual human immunodeficiency virus type 1 gp120 amino acids important for CD4 receptor binding. *J. Virol.* **64**, 5701–5707 (1990).
6. Pantophlet, R., Wilson, I.A. & Burton, D.R. Hyperglycosylated mutants of human immunodeficiency virus (HIV) type 1 monomeric gp120 as novel antigens for HIV vaccine design. *J. Virol.* **77**, 5889–5901 (2003).
7. Finzi, A. *et al.* Topological layers in the HIV-1 gp120 inner domain regulate gp41 interaction and CD4-triggered conformational transitions. *Mol. Cell* **37**, 656–667 (2010).
8. Kwong, P.D. *et al.* Structure of an HIV gp120 envelope glycoprotein in complex with the CD4 receptor and a neutralizing human antibody. *Nature* **393**, 648–659 (1998).
9. Kwong, P.D. *et al.* Structures of HIV-1 gp120 envelope glycoproteins from laboratory-adapted and primary isolates. *Structure* **8**, 1329–1339 (2000).
10. Huang, C.C. *et al.* Structure of a V3-containing HIV-1 gp120 core. *Science* **310**, 1025–1028 (2005).
11. Pancera, M. *et al.* Structure of HIV-1 gp120 with gp41-interactive region reveals layered envelope architecture and basis of conformational mobility. *Proc. Natl. Acad. Sci. USA* **107**, 1166–1171 (2010).
12. Lyumkis, D. *et al.* Cryo-EM structure of a fully glycosylated soluble cleaved HIV-1 envelope trimer. *Science* **342**, 1484–1490 (2013).
13. Stewart-Jones, G.B. *et al.* Trimeric HIV-1-env structures define glycan shields from clades A, B, and G. *Cell* **165**, 813–826 (2016).
14. Sanders, R.W. *et al.* A next-generation cleaved, soluble HIV-1 Env trimer, BG505 SOSIP.664 gp140, expresses multiple epitopes for broadly neutralizing but not non-neutralizing antibodies. *PLoS Pathog.* **9**, e1003618 (2013).
15. Julien, J.P. *et al.* Crystal structure of a soluble cleaved HIV-1 envelope trimer. *Science* **342**, 1477–1483 (2013).
16. Kwon, Y.D. *et al.* Crystal structure, conformational fixation and entry-related interactions of mature ligand-free HIV-1 Env. *Nat. Struct. Mol. Biol.* **22**, 522–531 (2015).
17. Garces, F. *et al.* Affinity maturation of a potent family of HIV antibodies is primarily focused on accommodating or avoiding glycans. *Immunity* **43**, 1053–1063 (2015).
18. Pancera, M. *et al.* Structure and immune recognition of trimeric pre-fusion HIV-1 Env. *Nature* **514**, 455–461 (2014).
19. Hu, G., Liu, J., Taylor, K.A. & Roux, K.H. Structural comparison of HIV-1 envelope spikes with and without the V1/V2 loop. *J. Virol.* **85**, 2741–2750 (2011).
20. Lee, J.H., Ozorowski, G. & Ward, A.B. Cryo-EM structure of a native, fully glycosylated, cleaved HIV-1 envelope trimer. *Science* **351**, 1043–1048 (2016).
21. Liu, J., Bartesaghi, A., Borgnia, M.J., Sapiro, G. & Subramaniam, S. Molecular architecture of native HIV-1 gp120 trimers. *Nature* **455**, 109–113 (2008).
22. Munro, J.B. *et al.* Conformational dynamics of single HIV-1 envelope trimers on the surface of native virions. *Science* **346**, 759–763 (2014).
23. Harris, A. *et al.* Trimeric HIV-1 glycoprotein gp140 immunogens and native HIV-1 envelope glycoproteins display the same closed and open quaternary molecular architectures. *Proc. Natl. Acad. Sci. USA* **108**, 11440–11445 (2011).
24. Scharf, L. *et al.* Broadly neutralizing antibody 8ANC195 recognizes closed and open states of HIV-1 Env. *Cell* **162**, 1379–1390 (2015).

25. Walker, L.M. *et al.* Broad neutralization coverage of HIV by multiple highly potent antibodies. *Nature* **477**, 466–470 (2011).
26. Li, Y. *et al.* Broad HIV-1 neutralization mediated by CD4-binding site antibodies. *Nat. Med.* **13**, 1032–1034 (2007).
27. Walker, L.M. *et al.* Broad and potent neutralizing antibodies from an African donor reveal a new HIV-1 vaccine target. *Science* **326**, 285–289 (2009).
28. Huang, J. *et al.* Broad and potent HIV-1 neutralization by a human antibody that binds the gp41-gp120 interface. *Nature* **515**, 138–142 (2014).
29. Alsahafi, N., Debbeche, O., Sodroski, J. & Finzi, A. Effects of the I559P gp41 change on the conformation and function of the human immunodeficiency virus (HIV-1) membrane envelope glycoprotein trimer. *PLoS One* **10**, e0122111 (2015).
30. Xiang, S.H., Doka, N., Choudhary, R.K., Sodroski, J. & Robinson, J.E. Characterization of CD4-induced epitopes on the HIV type 1 gp120 envelope glycoprotein recognized by neutralizing human monoclonal antibodies. *AIDS Res. Hum. Retroviruses* **18**, 1207–1217 (2002).
31. Ding, S. *et al.* A highly conserved gp120 inner domain residue modulates Env conformation and trimer stability. *J. Virol.* **90**, 8395–8409 (2016).
32. Rizzuto, C.D. *et al.* A conserved HIV gp120 glycoprotein structure involved in chemokine receptor binding. *Science* **280**, 1949–1953 (1998).
33. Zhou, T. *et al.* Structural definition of a conserved neutralization epitope on HIV-1 gp120. *Nature* **445**, 732–737 (2007).
34. Zhou, T. *et al.* Structural basis for broad and potent neutralization of HIV-1 by antibody VRC01. *Science* **329**, 811–817 (2010).
35. Zhou, T. *et al.* Structural repertoire of HIV-1-neutralizing antibodies targeting the CD4 supersite in 14 donors. *Cell* **161**, 1280–1292 (2015).
36. Li, Y. *et al.* HIV-1 neutralizing antibodies display dual recognition of the primary and coreceptor binding sites and preferential binding to fully cleaved envelope glycoproteins. *J. Virol.* **86**, 11231–11241 (2012).
37. Wu, X. *et al.* Focused evolution of HIV-1 neutralizing antibodies revealed by structures and deep sequencing. *Science* **333**, 1593–1602 (2011).
38. Georgiev, I.S. *et al.* Delineating antibody recognition in polyclonal sera from patterns of HIV-1 isolate neutralization. *Science* **340**, 751–756 (2013).
39. Xing, L. *et al.* Distinct cellular receptor interactions in poliovirus and rhinoviruses. *EMBO J.* **19**, 1207–1216 (2000).
40. Neumann, E., Moser, R., Snyers, L., Blaas, D. & Hewat, E.A. A cellular receptor of human rhinovirus type 2, the very-low-density lipoprotein receptor, binds to two neighboring proteins of the viral capsid. *J. Virol.* **77**, 8504–8511 (2003).
41. Xing, L. *et al.* Structural and functional analysis of integrin α_2I domain interaction with echovirus 1. *J. Biol. Chem.* **279**, 11632–11638 (2004).
42. Wang, H. *et al.* Cryo-EM structure of a CD4-bound open HIV-1 envelope trimer reveals structural rearrangements of the gp120 V1V2 loop. *Proc. Natl. Acad. Sci. USA* **113**, E7151–E7158 (2016).
43. Huang, C.C. *et al.* Structures of the CCR5 N terminus and of a tyrosine-sulfated antibody with HIV-1 gp120 and CD4. *Science* **317**, 1930–1934 (2007).
44. de Taeye, S.W. *et al.* Immunogenicity of stabilized HIV-1 envelope trimers with reduced exposure of non-neutralizing epitopes. *Cell* **163**, 1702–1715 (2015).

ONLINE METHODS

Sample preparation for electron microscopy analysis. DS-SOSIP.664, four-domain CD4, and PGT145 Fab were expressed and purified as described previously[16]. Purified DS-SOSIP.664 at 1 mg/ml was incubated with 20 μM of four-domain sCD4 for 16 h at room temperature; PGT145 Fab was then added at three-fold molar excess of the trimer concentration, and the sample was incubated for another 3–4 h before vitrification.

Specimen vitrification for cryo-EM. To avoid aggregation during vitrification, the sample was incubated with a small amount of dodecyl maltoside at a final concentration of 0.085 mM (2× below the critical micelle concentration). To prepare specimens for cryo-EM we applied 3 μL of sample to a freshly plasma-cleaned holey gold grid, allowed the sample to adsorb to the grid for 30 s, and then blotted the grids with filter paper and plunge-froze them in liquid ethane using the CP3 cryo-plunger (Gatan, Inc.) (20 °C, 85–90% relative humidity).

Cryo-EM data collection and raw-frame alignment. As summarized in **Table 1**, data were acquired using the Leginon system[45] installed on a Krios electron microscope operating at 300 kV, with a dose of ~86 $e^-/Å^2$ and an estimated defocus ranging from 1.0 to 4.0 μm underfocus (distributed in an approximately Gaussian manner and centered at 2.5 ± 0.8 μm). The dose was fractionated over 40 raw frames collected over a 10-s exposure time (250 ms per frame) on the Gatan K2 Summit direct detection device. A total of 1,900 such 'movies' were automatically collected over a span of four data collection sessions, recorded at a nominal magnification of 22,500×, corresponding to a pixel size of 1.1 Å at the specimen level. The individual frames were globally aligned using a GPU-enabled frame-alignment program (generously provided by Y. Cheng and X. Li)[46].

Image processing and refinement. Unless otherwise noted, all of the following image-processing steps were performed within the Appion pipeline[47,48]. The contrast transfer function for all micrographs was estimated with the GCTF package[49]. All micrographs were also manually masked with the "manual masking" tool in Appion to remove regions that were over gold and/or contained large amounts of disordered or aggregated particles. To obtain a clean stack of particles on which to perform the final refinement, we first performed an iterative stack cleaning procedure (described below). Particles were initially selected using DoG Picker[50] from 800 micrographs (**Supplementary Fig. 1a**). A phase-flipped, contrast-inverted, and 2× binned stack of 10,000 particles was created from these picked particles with a box size of 160 pixels and pixel size of 2.2 Å, and subjected to reference-free 2D alignment and clustering by CL2D[51] to obtain 256 2D classes. The classes were inspected visually, and 15 of these classes (representing different views) were used as templates to select particles over the entire set of micrographs using the template-picking algorithm in Appion[52,53]. After 2D alignment and clustering with CL2D and RELION[48] (outside of Appion) to eliminate class averages that did not display identifiable features (**Supplementary Fig. 1b**), 100,500 particles were retained for all subsequent analyses, which were done outside of Appion. A map of unliganded BG505 SOSIP.664 (EMD-5782), low-pass filtered to 60 Å, was used as the starting point of 3D classification/sorting to eliminate trimer particles that were not bound to both CD4 and PGT145, as well as to exclude badly formed particles. After two rounds of 3D classification separating the particles into four classes in the first round and three classes in the second round, the class that showed both PGT145 and CD4 bound (class I) (**Supplementary Fig. 1c**) was selected for 3D refinement in RELION (**Table 1** and **Supplementary Fig. 1d**,**e**). Automasking in RELION[54] yielded an 18-Å resolution map. We truncated the CD4 density from this map using the volume eraser tool in Chimera, and used the relion_mask_create program to make masks that extended from this CD4-truncated map. We then carried out 3D refinement with these manual masks, which resulted in maps with incrementally truncated density for the bound CD4 with resolutions of 11 Å (mask 1) and 9 Å (mask 2) (**Supplementary Fig. 1e**). Next, we carried out dose fractionation by incrementally excluding movie frames; the best resolutions of 9 Å (mask 1) and 7.5 Å (mask 2) were achieved for the two maps that were generated with masks truncated at different lengths, by using the first 30 frames, which corresponded to a total dose of ~51 $e^-/Å^2$. In a second masking strategy we generated masks extending from the 3D map from class I (**Supplementary Fig. 1c**) followed by auto-refine within RELION using these manual masks, resulting in a best resolution of 6.8 Å after post-processing within RELION (**Supplementary Fig. 1e**). This 6.8-Å-resolution reconstruction showed the best-resolved density for the bound four-domain CD4 molecule. This map was used for all model fitting unless otherwise noted.

Model fitting. First, all HIV-1 Env soluble trimer models available in PDB were fitted onto the 7.5-Å cryo-EM map (**Supplementary Table 1**). Next, each fitted trimer was separated into its gp120-gp41 protomers, and the protomers were fitted to optimize map-to-model correlation. The trimer with the optimal fit was assembled through combination of the protomers that fit the map with highest correlation. On examination of the protomers, all three of which came from PDB 5ACO, it was found that the protomers were missing residues 59–67 in the gp120 chains. This stretch of residues was added back into each of the protomers by superposition with the trimer in PDB 5FYL[13] and grafting of residues 57–70 from each protomer of PDB 5FYL to each equivalent protomer of the fitted trimer. This resulted in a small increase in map-to-model correlation from 0.84 to 0.85. Finally, the fits of the protomers were optimized within the 6.8-Å cryo-EM map. Once the fit of the trimer to the map had been optimized, the coordinates of free PGT145 (PDB 3U1S)[56] were fit to the density visible in the map near the V1V2 region of the trimer. The Fab was first fit as a whole; then, fits for the variable and constant domains were optimized separately to maximize map-to-model correlation. Two orientations of the antibody Fab fragment, rotated by 180° along the longitudinal axis of the Fab, were tested, and the orientation that fit with higher correlation (0.75) was also visually found to fit better to the map (**Supplementary Fig. 2**) compared with the Fab orientation that fit the electron microscopy map with reduced correlation (0.66). To fit CD4, we used an approach similar to that used for the trimer, using all the PDB deposits containing CD4 (**Supplementary Table 2**). For gp120-bound CD4, we superposed the gp120 in the gp120–CD4 complex with the gp120 protomer in the trimer that had its outer-domain CD4-binding loop facing the CD4 density in the cryo-EM map. We designated the resulting orientation as the 'post-fusion' orientation of CD4. For CD4 structures that were not bound to gp120, CD4 residues 2–176 were superimposed on residues 2–176 of CD4 from PDB 2NY4 that had already been placed in the post-fusion orientation. From this starting position, we fit each CD4 molecule using rigid-body docking within Chimera[55] (**Supplementary Table 2** and **Fig. 4c**). Following model fitting, the PGT145-trimer and CD4-trimer interfaces were minimized using the steepest descent protocol in Chimera, and the interactive areas were optimized by varying side chain rotamer conformations. The 7.5-Å map obtained with Mask2 in RELION auto-refine (**Supplementary Fig. 1e**) showed better definition of the glycan density around the trimer, and was used to place the glycans.

Structural analyses. To calculate the relative orientations of the CD4-bound protomers in the single CD4-bound Env trimer structure, we first superposed all trimer structures with the PDB entries listed in **Supplementary Table 1** to the single-CD4-bound structure, by aligning a protomer of each trimer to the protomer of the single-CD4-bound Env trimer that did not contact CD4. For trimers where each protomer had been determined independently (i.e., where electron microscopy maps were refined using C1 symmetry or where the entire trimer was part of one crystallographic asymmetric unit), each protomer was fit to the protomer of the single CD4-bound Env trimer that did not contact CD4. From this starting orientation, for each pairwise comparison between the single CD4-bound trimer and an Env trimer from the PDB, the rotation and the translation needed to superpose the two CD4 contacting protomers to the respective protomers of the aligned Env trimer were calculated (**Fig. 4c**). All superpositions were performed using the Superpose module[57] within the CCP4 suite[58], and rotation angles were obtained with Superpose (MATLAB, The MathWorks Inc.) and Origin (OriginLab).

For estimating surface area buried at the interfaces between trimer and CD4, starting from the Env trimers listed in **Supplementary Table 1** that had been fitted to the EM density map, trimers missing any of the following CD4 contacting residues were removed: 281, 368, 371, 280, 428, 62, 64, 65, 66, or 207. This resulted in seven Env trimer structures. Similarly, for CD4, starting from **Supplementary Table 2** with CD4 structures that had been fitted to the EM density map, CD4 missing any of the following Env trimer contacting residues were removed: 20, 21, 22, 40, 43, or 64. This resulted in 29 CD4 structures. Complex structures for all pairwise Env trimer–CD4 combinations were minimized using Chimera[55] (only CD4 D1 domain and Env residues that are 10 Å within CD4 were allowed

to move). The side chain rotamers of the interface residues were further refined using SCAP[59]. Buried surface areas were calculated using PISA[60].

To define the CD4 supersite that is targeted by CD4-BS antibodies on the pre-fusion closed HIV-1 Env trimer, we superposed PDB coordinates of HIV-1 gp120 in complex with CD4-BS antibodies isolated from 14 human donors[35] onto the BG505.SOSIP (PDB 4TVP) by aligning the outer domain residues 255:392, 412:422 and 437:459. The CD4 supersite for antibodies was defined as a set of HIV-1 Env atoms that are within 5.5 Å of docked CD4-BS antibodies, including the VH1-2 germline-derived VRC01-class antibodies, the VH1-46 germline-derived 8ANC131 class antibodies and the CDR H3-dominated antibodies (VRC13, VRC16, CH103, and HJ16). In addition to the previously defined primary antibody contact region on gp120, the CD4 supersite for CD4-BS antibodies also extended to the neighboring gp120 protomer in the trimeric pre-fusion closed Env and overlapped with CD4-BS2. Electrostatic potential molecular surfaces for antibodies and HIV-1 gp120 were generated with the APBS and PDB2PQR server (http://nbcr-222.ucsd.edu/pdb2pqr_2.1.1/).

Molecular dynamics simulation. A model of the structure of the HIV-1 BG505-SOSIP.664 trimer with a single CD4 molecule bound was subjected to an all-atom, isobaric-isothermal (1 atm, 310 K) MD simulation. The simulation was done with the AceMD[61] program (v.3212) on the Biowulf Linux cluster at the NIH, Bethesda, MD (http://biowulf.nih.gov). The complex was explicitly solvated with TIP3P water, neutralized through the addition of counterions (Na^+, Cl^- to 0.15 M), with periodic boundary conditions applied. Electrostatic interactions were calculated using the particle-mesh Ewald summation with grid spacing of 1 Å along with a 9-Å cutoff. The CHARMM27 force field was used[61] for protein. The system was energy minimized, warmed to 310 K, and submitted to a production run. We implemented a 4-fs integration-time step by making use of a hydrogen mass repartitioning scheme, and we collected data for 668 ns. Langevin dynamics were used to maintain temperature, and a Berendsen barostat was used to control pressure.

Sequence conservation analysis. Sequence alignment of a segment of the C1 region (centered around the α1-helix) and of the C2 region (a segment of the β3-β4 loop) of the gp120 inner domain from the all the available group M HIV-1 and SIVcpz isolates (including both subtypes A–K and recombinant forms) was obtained from the Los Alamos HIV database (http://www.hiv.lanl.gov). The sequence logo was created with WebLogo (http://weblogo.berkeley.edu). The height of each stack indicates the degree of conservation for each residue; the relative height of each letter within an individual stack represents the frequency of the indicated amino acid at that site.

Mutagenesis, protein expression, and purification. Site-directed mutagenesis was carried out with the QuikChange II site-directed mutagenesis kit (Agilent Technologies). The BG505-SOSIP.664 trimer was expressed by cotransfection of the relevant plasmid (a kind gift of John P. Moore) with a plasmid expressing the cellular protease furin into HEK293FS cells. Cell-free supernatants were harvested after 7 d, passed through a 0.22-μm filter, and loaded onto a *Galanthus nivalis* lectin column (Vector laboratories). After repeated washing with PBS, bound proteins were eluted with 1 M methyl α-D-mannopyranoside in PBS, and then subjected to dialysis toward PBS. Dialyzed samples were concentrated to 2 ml using Amicon Ultra-15 centrifugal filter units (MWCO 50,000, Millipore) and applied to a PBS pre-equilibrated Superdex 200 column. The peak corresponding to the trimeric form was collected and concentrated, after which sample underwent a second round of Superdex 200 purification. Finally, purified trimers were concentrated to 0.5–1 mg/ml and stored at −80 °C. Monomeric HIV-1 BG505-T332N gp120 and BaL gp120 (gene synthesized by GeneArt) were expressed in HEK293FS cells. After 7 d, the supernatants were harvested and passed through a 0.22-μm filter. We purified gp120 by loading filtered supernatants onto a lectin column as described above. The eluted proteins were concentrated with Amicon Ultra-15 centrifugal filter units (MWCO 10,000, Millipore) and applied to a Superdex 200 column. DS-SOSIP.664-based trimers were purified as described previously[16]. Briefly, cell-free supernatants were loaded onto a VRC01 or 2G12 affinity column and subjected to gel filtration. The trimeric form was collected and passed through a 447-52D affinity column for negative selection. Further cleanup was done with a column of anti-V3 (1006-15D, 2219, 2557, 2558, 3074, 50.1).

Expression of full-length HIV-1 gp160 or CD4. The full-length *CD4* gene and the gene encoding gp160 from BG505-T332N and BaL (both from Edward Berger) were mutagenized as described above for the SOSIP trimer. HEK293T cells were used to express CD4 or gp160 on the cell-surface membrane. The cells were seeded into six-well plates at 300,000 cells per well in 2 ml of DMEM containing 10% FBS (DMEM 10%). After overnight incubation at 37 °C in a humidified atmosphere with 5% CO_2, the culture medium was replaced with 1.5 ml of fresh 10% DMEM. We prepared DNA-FuGENE 6 complex by mixing 2 μg of DNA with 10 μl of FuGENE 6 Transfection Reagent (Promega) in Opti-MEM (Gibco) to a final volume of 150 μl and incubated it for 15 min at room temperature (RT). The cells were transfected by dropwise addition of the DNA–FuGENE 6 complex to each well, and were harvested after 48–60 h. The same protocol was used for CD4 expression on the surface membrane of Cf2Th/syn-CCR5 cells (AIDS Reagent Program).

Flow cytometry. HEK293T cells expressing CD4 or gp160 were harvested by mechanical shaking and pipetting, washed with PBS, and incubated with anti-CD4 or anti-gp120 (5 μg/ml) or serially diluted human Fc-chimeric CD4-immunoglobulin (produced in HEK293FS cells; plasmid provided by Michael Farzan) at RT for 30 min. After being washed with PBS twice, the cells were incubated with PE-conjugated sheep anti-mouse IgG (Sigma) or goat anti-human IgG (Southern Biotech) at RT for 15 min. The cells were then washed once with PBS, fixed in 2% paraformaldehyde and analyzed on a BD FACSCanto (BD Biosciences). Data analysis was done with the FlowJo software.

Pseudovirus preparation and infectivity assays. Viral pseudoparticles expressing wild-type or mutated gp160 from HIV-1 BG505-T332N or BaL were produced in HEK293T cells by cotransfection of Env-expressing plasmids together with a backbone plasmid, $pSG3^{\Delta env}$, expressing a full-length HIV-1 clone with a defective Env gene. To produce the pseudoparticles, we mixed 2 μg of each Env-expressing plasmid and 4 μg of the backbone plasmid in Opti-MEM medium (Gibco), added 24 μl of FuGENE 6 transfection reagent, and incubated the mixture for 15 min at RT. DNA–FuGENE 6 complex was then added to the cells and incubated overnight at 37 °C. After the culture medium had been replaced with 2 ml of fresh 10% DMEM, the cells were incubated for 48 h and the supernatants containing the pseudoviruses were harvested by centrifugation. For pseudovirus infection, TZM-bl cells (AIDS Reagent Program) were harvested and seeded into 96-well flat-bottom plates at 10,000 cells per well in 100 μl 10% DMEM. After 30 min at 37 °C, the pseudovirus stock (normalized to 1 ng of $p24_{GAG}$ protein per mutant) was added to the cells in a total volume of 200 μl/well. Reporter gene activation was detected 2 d later with a luciferase assay kit (Promega) with a luminometer (PerkinElmer). Relative light units (RLU) were recorded, and the final values were normalized against the values obtained with the wild-type Env set at 100%. All the samples were tested in duplicate wells.

We produced pseudoviruses expressing firefly luciferase by cotransfecting Env-expressing plasmids (wild-type BaL or BG505-T332N) together with a backbone plasmid, $pNL4\text{-}3.Luc.R^-E^-$ (AIDS Reagent Program), at a ratio of 1:1. Supernatants containing pseudoviurses were harvested by centrifugation after 48 h of incubation. We prepared target cells by transfecting wild-type or mutated CD4-expressing plasmids to Cf2Th/syn-CCR5 cells. After incubation for 24 h, the cells were harvested and seeded to 96-well flat-bottom plates at 10,000 cells per well in 100 μl of 10% DMEM. Pseudovirus stocks were added to the cells to a total volume of 200 μl/well. The reporter gene activity was detected 2 d later with a luciferase assay kit (Promega) and expressed as RLU. Serial dilutions of the wild-type CD4 plasmid were used to generate a reference curve, which allowed us to extrapolate accurate infectivity values for each mutant on the basis of expression levels, as measured by flow cytometry using mAb OKT4. All samples were performed in duplicate.

Enzyme immunoassays. All the antibodies and envelope proteins used in ELISA experiments were diluted in 0.02% casein in PBS. All samples were washed three times after each step with 1× wash buffer (R&D Systems). For assessment of sCD4 binding to the BG505 SOSIP.664 trimers or gp120 monomers, 96-well ELISA plates (Corning) were coated with 2 μg/ml mAb 2G12 at 4 °C overnight. After blocking with 0.2% casein in PBS, purified trimers or monomers (2 μg/ml) were added and incubated for 2 h at RT. After washing, serially diluted four-domain sCD4 (R&D Systems) was added and incubated for 1 h at RT. After washing, the

doi:10.1038/nsmb.3382

samples were incubated with biotin-labeled mAb OKT4 (eBioscience; 13-0048-82) for 1 h; after additional washing, horseradish peroxidase (HRP)-conjugated streptavidin (R&D Systems; DY998) was added for 1 h at RT. The reaction was revealed by incubation with the appropriate substrate for 10 min before addition of the stop solution. Light absorption was measured at a wavelength of 450 nm. All samples were tested in duplicate or triplicate wells. To evaluate antibody binding, we coated ELISA plates with 5 µg/ml of an anti-gp120 C-terminus hyperimmune sheep antiserum (Aalto Bio Reagents; D7324) for monomeric gp120 or with 0.5 µg/ml of rabbit anti-His tag antiserum for trimers (GenScript; A00174). Monomeric gp120s or trimers were captured on the plates, and various antibodies to gp120 (0.5–5 µg/ml or serial dilutions starting from 5–20 µg/ml) were added to the wells and incubated for 1 h, and subsequently for another hour with HRP-conjugated goat anti-human IgG (Sigma; A8419) at RT. The subsequent steps were the same as described above. For all the mutants, relative binding compared to the wild type was calculated. To evaluate antibody binding to DS-SOSIP.664, we coated the ELISA plate with 10 µg/ml lectin from *Galanthus nivalis* (Sigma). DS-SOSIP.664 proteins were added at 1 µg/ml for capture. Various antibodies to gp120 were tested at 1–5 µg/ml or with serial dilutions starting from 5–20 µg/ml.

Surface plasmon resonance analyses. Single-cycle kinetics analysis of two-domain sCD4 binding to the BG505 SOSIP.664 and DS-SOSIP.664 trimers was performed at 20 °C on a Biacore T200 (GE Healthcare) as described previously[16]. Briefly, mAb 2G12 was immobilized onto four flow cells of a CM5 sensor to ~2,000 response units (RU) using the amine-coupling method. Purified BG505 SOSIP.664 trimers were injected to two sample flow cells at a flow rate of 5 µl/min for 2 min, and captured to 300–400 RU. The other two flow cells were left blank as a reference. Series dilutions of sCD4 (180 nM, 90 nM, 45 nM, 22.5 nM, 11.25 nM) were injected into both the reference and sample flow cells at 50 µl/min in a single cycle, starting from the lowest concentration. Ten minutes of dissociation phase was allowed after the last sCD4 injection. We carried out the same injections with HBS-EP buffer to obtain a reference curve. Data were fitted to a 1:1 Langmuir model with Biacore T200 evaluation software. By SPR analysis, we verified that the differential CD4 binding of CD4-BS2 mutants was not due to altered binding to mAb 2G12 (data not shown).

CCR5-binding assay. Cf2Th/syn-CCR5 cells, which express high levels of CCR5 on their surface membrane, were used to assess binding of soluble BG505-SOSIP.664 trimers or BaL gp120 monomers to CCR5. The cells were harvested at ~80% confluence with enzyme-free cell-dissociation buffer (Gibco). His-tagged BG505-SOSIP.664 trimers or BaL gp120 monomers were pre-incubated with or without two-domain sCD4 for 1 h at 4 °C and incubated with the cells for 1 h at 4 °C, and then washed with PBS. For BG505-SOSIP.664 trimers, PE-conjugated mouse anti-His tag (Miltenyi Biotec; 120-003-741) was added to the cells for 1 h at 4 °C. For gp120 monomers, D7324 was added to the cells for 1 h at 4 °C, and then incubated for 15 min with CF™ 488A-conjugated chicken anti-goat antibody (Sigma; SAB4600028). The cells were then washed once with PBS, fixed with 2% PFA, and analyzed on a BD FACSCanto instrument. The specificity of binding was assessed by abrogation of the signal with an anti-CCR5 mAb (Becton Dickinson; 555991). Data analysis was done with the FlowJo software.

Structure alignments and figures. All graphs were plotted using Graphpad Prism, and structural figures were displayed using Pymol (https://www.pymol.org). PDB IDs are referenced in individual figures.

Data availability. The 7.5-Å and 6.8-Å cryo-EM maps have been deposited under accession code EMD-8427. Fitted coordinates have been deposited under accession code PDB 5U1F. Primary data are available upon request from the corresponding author.

45. Suloway, C. *et al.* Automated molecular microscopy: the new Leginon system. *J. Struct. Biol.* **151**, 41–60 (2005).
46. Li, X. *et al.* Electron counting and beam-induced motion correction enable near-atomic-resolution single-particle cryo-EM. *Nat. Methods* **10**, 584–590 (2013).
47. Lyumkis, D. *et al.* Automation in single-particle electron microscopy: connecting the pieces. *Methods Enzymol.* **483**, 291–338 (2010).
48. Lander, G.C. *et al.* Appion: an integrated, database-driven pipeline to facilitate EM image processing. *J. Struct. Biol.* **166**, 95–102 (2009).
49. Zhang, K. Gctf: real-time CTF determination and correction. *J. Struct. Biol.* **193**, 1–12 (2016).
50. Voss, N.R., Yoshioka, C.K., Radermacher, M., Potter, C.S. & Carragher, B. DoG Picker and TiltPicker: software tools to facilitate particle selection in single particle electron microscopy. *J. Struct. Biol.* **166**, 205–213 (2009).
51. Sorzano, C.O.S. *et al.* A clustering approach to multireference alignment of single-particle projections in electron microscopy. *J. Struct. Biol.* **171**, 197–206 (2010).
52. Roseman, A.M. Particle finding in electron micrographs using a fast local correlation algorithm. *Ultramicroscopy* **94**, 225–236 (2003).
53. Roseman, A.M. FindEM—a fast, efficient program for automatic selection of particles from electron micrographs. *J. Struct. Biol.* **145**, 91–99 (2004).
54. Scheres, S.H.W. RELION: implementation of a Bayesian approach to cryo-EM structure determination. *J. Struct. Biol.* **180**, 519–530 (2012).
55. Pettersen, E.F. *et al.* UCSF Chimera—a visualization system for exploratory research and analysis. *J. Comput. Chem.* **25**, 1605–1612 (2004).
56. McLellan, J.S. *et al.* Structure of HIV-1 gp120 V1/*V2* domain with broadly neutralizing antibody PG9. *Nature* **480**, 336–343 (2011).
57. Krissinel, E. & Henrick, K. Secondary-structure matching (SSM), a new tool for fast protein structure alignment in three dimensions. *Acta Crystallogr. D Biol. Crystallogr.* **60**, 2256–2268 (2004).
58. Winn, M.D. *et al.* Overview of the CCP4 suite and current developments. *Acta Crystallogr. D Biol. Crystallogr.* **67**, 235–242 (2011).
59. Xiang, Z. & Honig, B. Extending the accuracy limits of prediction for side-chain conformations. *J. Mol. Biol.* **311**, 421–430 (2001).
60. Krissinel, E. & Henrick, K. Inference of macromolecular assemblies from crystalline state. *J. Mol. Biol.* **372**, 774–797 (2007).
61. Harvey, M.J., Giupponi, G. & Fabritiis, G.D. ACEMD: accelerating biomolecular dynamics in the microsecond time scale. *J. Chem. Theory Comput.* **5**, 1632–1639 (2009).

Corrigendum: Quaternary contact in the initial interaction of CD4 with the HIV-1 envelope trimer

Qingbo Liu, Priyamvada Acharya, Michael A Dolan, Peng Zhang, Christina Guzzo, Jacky Lu, Alice Kwon, Deepali Gururani, Huiyi Miao, Tatsiana Bylund, Gwo-Yu Chuang, Aliaksandr Druz, Tongqing Zhou, William J Rice, Christoph Wigge, Bridget Carragher, Clinton S Potter, Peter D Kwong & Paolo Lusso

***Nat. Struct. Mol. Biol.* 24, 370–378 (2017); published online 20 February 2017; corrected after print 27 April 2017**

In the version of this article initially published, funding information for B.C. and C.S.P. was missing NIH grant S10 OD019994-01. In addition, there was an incorrect comma in the introduction (after "glycoprotein" in the sentence "Upon binding to the primary cellular receptor, CD4, the external gp120 Env glycoprotein undergoes major conformational changes…") that has been removed. The errors have been corrected in the HTML and PDF versions of the article.